



PAPER



Cite this: *Phys. Chem. Chem. Phys.*,
2018, 20, 19647

Understanding mode-specific dynamics in the local mode representation

Hongwei Song * and Minghui Yang 

Mode specificity is a main characteristic of transition state control of reaction dynamics. The normal mode representation has been widely employed to describe the mode specificity in elementary chemical reactions. However, spectroscopists have demonstrated that the local mode representation has advantages in analyzing the overtone and combination band spectra. In this work, the mode-specific reaction dynamics between the hydrogen atom and the molecules H_2S and H_2O is studied using a full-dimensional quantum scattering model in the $(2 + 1)$ Radau–Jacobi coordinates. The mode specificities in the reactions that violates our physical intuition in the normal mode representation are well rationalized in the local mode representation. The energy flow between different XH bonds resulting from the intramolecular interaction and/or intermolecular interaction is unveiled, together with its impacts on dynamics of the abstraction and exchange reactions.

Received 22nd May 2018,
Accepted 10th July 2018

DOI: 10.1039/c8cp03240h

rsc.li/pccp

1. Introduction

An activated chemical reaction is usually controlled by the transition state.¹ One main characteristic of transition state control of reaction dynamics is so called mode specificity, namely the dependence of reactivity on the excitation of different reactant vibrational modes. Studying mode specific dynamics of elementary bimolecular reactions would advance understanding of intrinsic nature of chemical reactions and provide theoretical and experimental foundations for controlling and utilizing the reactions.^{2–4} Thanks to the rapid development of laser techniques, it has nowadays become feasible to prepare reactant molecules in a single quantum state to investigate mode specificity and bond selectivity.^{5–11}

The normal mode representation has been widely employed to describe molecular vibrational motions, in which each normal mode acts like a simple harmonic oscillator and behaves as a concerted motion of many atoms. The mode specificity in molecular reaction dynamics is unsurprisingly reported in the normal mode representation.^{12–19} In this regard, comprehensive studies have proved that fundamental excitations of the symmetric and/or antisymmetric stretching modes of the reactants $\text{H}_2\text{O}/\text{CH}_4$ promote remarkably the reactivity of the reactions $\text{X} + \text{H}_2\text{O}/\text{CH}_4$ ($\text{X} = \text{H}, \text{F}, \text{O}(^3\text{P}), \text{Cl}$ and OH) while excitation of the bending mode leads to a weaker enhancement effect.^{20–42} This can be easily understood by considering the coupling between the reactant normal mode

vector and the reaction coordinate vector at the transition state, as has been implemented by the sudden vector projection model.¹⁵ However, Fu *et al.*³² demonstrated that for the $\text{H} + \text{H}_2\text{O} \rightarrow \text{H}_2 + \text{OH}$ reaction first overtone excitation of the symmetric stretching mode (200) of the reactant H_2O promotes the reactivity much more than excitation of the antisymmetric stretching mode (002) while the efficiency of exciting the state (200) on promoting the reaction is comparable to exciting the combination band (101). These dynamical features in the $\text{H} + \text{H}_2\text{O} \rightarrow \text{H}_2 + \text{OH}$ reaction obviously violate one's physical intuition since the concerted motions of the two hydrogen atoms in the two stretching modes are expected to have similar dynamics effect. Impressively, they pointed out that (200) and (101) states in the normal mode notation correspond to the (200) and (200) states in the local mode notation and attempted to rationalize these dynamical features in the local representation.³² Very recently, Zhang's⁴³ and Guo's^{44,45} groups investigated the state-to-state dynamics of the prototypical $\text{H} + \text{H}_2\text{O} \rightarrow \text{H}_2 + \text{OH}$ reaction and argued that the vibration energy deposited in the spectator bond OH of H_2O is sequestered during the reaction, indicating a good local mode character of the reactant H_2O .

Although the concept of the normal mode is really ingrained in describing molecular vibrations, it has been demonstrated in the past several decades that the local mode representation has advantages in analyzing the overtone and combination band spectra, especially for X–H vibrations.⁴⁶ In the local mode representation, the stretching vibration are described by anharmonic oscillators localized on individual X–H bond with harmonic inter-bond coupling. In association with the aforementioned dynamics behavior in the $\text{H} + \text{H}_2\text{O}$ reaction,^{43,44} it prompts us to study mode-specific dynamics in the local

State Key Laboratory of Magnetic Resonance and Atomic and Molecular Physics,
Wuhan Institute of Physics and Mathematics, Chinese Academy of Sciences,
Wuhan 430071, China. E-mail: hwsong@wipm.ac.cn

mode representation. The local mode treatment would provide a new perspective to understand reaction mechanisms of elementary chemical reactions.

In this work, time-dependent quantum wave packet calculations will be carried out to study the reaction dynamics between the hydrogen atom and the molecules H_2S and H_2O . The reactants H_2S and H_2O are both typical local mode molecules and the local mode character of H_2S is slightly stronger than H_2O . The aim in this paper is twofold: (1) gain a comprehensive understanding of the mode specificity in elementary chemical reactions involving typical local mode molecules; (2) unveil the influence of the intramolecular interaction and/or the intermolecular interaction on the dynamics of reactions between the hydrogen atom and the molecules H_2S and H_2O . The accurate *ab initio*-based global potential energy surfaces (PESs) developed by Li *et al.*⁴⁷ for the H_3O system and by Lu *et al.*⁴⁸ for the H_3S system are employed in the dynamics calculations. They are both generated by fitting a large number of data points sampled over a relevant configuration space using the permutation invariant polynomial-neural network method.^{47,49} Although the PES of the H_3O system used in this work is different from the YZCL2 PES⁵⁰ employed by Fu *et al.*, they are, however, expected to give consistent dynamic results.^{47,51} Thus, we do not repeat the calculations on the $\text{H} + \text{H}_2\text{O}$ reaction and yet carry out further dynamics calculations in the (2 + 1) Radau–Jacobi coordinates to explore the effect of the intramolecular interaction and/or the intermolecular interaction on the reaction dynamics. Schematic diagrams of the reaction paths for the two reactions are shown in Fig. 1. Both of the two reactions proceed through two reaction channels: abstraction channel and exchange channel. For the abstraction channel, the $\text{H} + \text{H}_2\text{S}$ reaction presents an early barrier while the $\text{H} + \text{H}_2\text{O}$ reaction has a late barrier. The paper is organized as follows. Section II outlines the theoretical methodologies on the quantum dynamics and the local mode

representation, followed by results and discussions in Section III. The conclusions are supplied in Section IV.

II. Theory

IIA. Quantum dynamics

In order to introduce the local mode representation, the (2 + 1) Radau–Jacobi coordinates are employed. Fig. 2 depicts (2 + 1) Radau–Jacobi coordinates, in which ρ is the distance from the center of mass (X) of BCD to the atom A, r_1 and r_2 are the distances from the canonical center (O) to the atoms A and B, respectively.

The canonical center is defined by $|\overrightarrow{OY}|^2 = |ZY| \cdot |XY|$, where Y is the center of mass of BC. The full-dimensional Hamiltonian in the reactant (2 + 1) Radau–Jacobi coordinates can be written as ($\hbar = 1$ thereafter):

$$\hat{H} = -\frac{1}{2\mu_\rho} \frac{\partial^2}{\partial \rho^2} - \frac{1}{2\mu_{r_1}} \frac{\partial^2}{\partial r_1^2} - \frac{1}{2\mu_{r_2}} \frac{\partial^2}{\partial r_2^2} + \frac{(\hat{J}_{\text{tot}} - \hat{J})^2}{2\mu_\rho \rho^2} + \frac{\hat{j}_1^2}{2\mu_1 r_1^2} + \frac{\hat{j}_2^2}{2\mu_2 r_2^2} + \hat{V}(\rho, r_1, r_2, \theta_1, \theta_2, \varphi), \quad (1)$$

where μ_ρ , μ_{r_1} and μ_{r_2} are reduced masses and defined as $\mu_\rho = \frac{m_A(m_B + m_C + m_D)}{m_A + m_B + m_C + m_D}$, $\mu_{r_1} = m_B$ and $\mu_{r_2} = m_C$. \hat{j}_1 is the angular momentum operator with respect to r_1 , \hat{j}_2 is the angular momentum operator with respect to r_2 , and $\hat{J} = \hat{j}_1 + \hat{j}_2$ is the angular momentum operator of BCD. \hat{J}_{tot} denotes the total angular momentum operator of the system. \hat{V} is the potential energy operator of the system.

The parity ε adapted wave function is expanded as:

$$\psi^{J_{\text{tot}} M \varepsilon}(\vec{\rho}, \vec{r}_1, \vec{r}_2) = \sum_{n, \nu_1, \nu_2, j, K} C_{n\nu_1\nu_2 j K}^{J_{\text{tot}} M \varepsilon} u_n^{\nu_1 \nu_2}(\rho) \phi_{\nu_1}(r_1) \phi_{\nu_2}(r_2) \Phi_{j K}^{J_{\text{tot}} M \varepsilon}(\vec{\rho}, \hat{r}_1, \hat{r}_2), \quad (2)$$

where n represents the translational basis index, ν_1 and ν_2 are the vibrational basis indices along the radical coordinates r_1 and r_2 and the composite index j denotes (j_1, j_2, J). M is the projection of the total angular momentum on the space-fixed z axis and K is its projection on the body-fixed (BF) z axis.

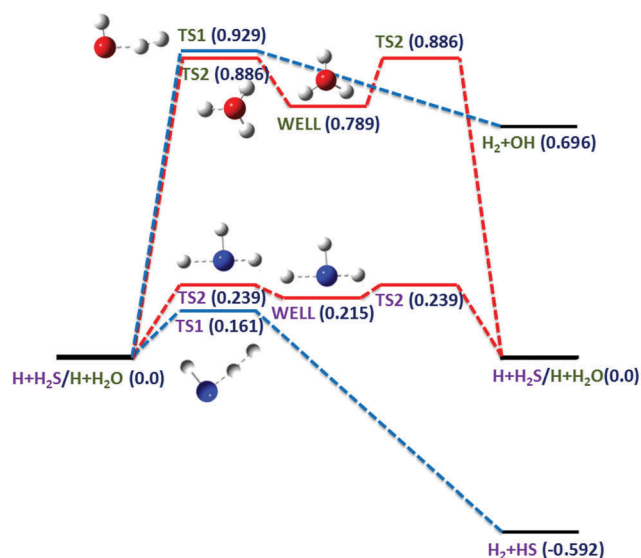


Fig. 1 Schematic diagrams of the reaction paths for the $\text{H} + \text{H}_2\text{S}$ and $\text{H} + \text{H}_2\text{O}$ reactions. Energies are given in eV.

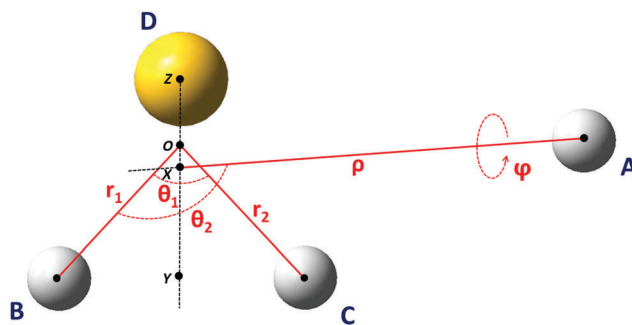


Fig. 2 The six-dimensional reactant (2 + 1) Radau–Jacobi coordinates for the $\text{A} + \text{BCD}$ reaction.

The BF z axis is defined along the coordinate ρ . The dependence of the translational basis function $u_n^{\nu_1\nu_2}$ on ν_1 and ν_2 is caused by the employment of an L-shaped grid.⁵² In the calculations, $u_n^{\nu_1\nu_2}$ is chosen as sine functions, ϕ_{ν_i} are constructed from the corresponding one-dimensional (1D) reference Hamiltonians that are defined as

$$\hat{h}_i(r_i) = -\frac{1}{2\mu_{r_i}} \frac{\partial^2}{\partial r_i^2} + V^{\text{ref}}(r_i), \quad i = 1, 2 \quad (3)$$

where $V^{\text{ref}}(r_i)$ are the corresponding 1D reference potentials along the coordinates r_i with the other coordinates fixing at the equilibrium geometry in the reactant asymptote. $\Phi_{JK}^{JM\epsilon}$ in eqn (3) is the parity-adapted total angular momentum eigenfunction in the BF frame, which can be expressed as

$$\begin{aligned} \Phi_{JK}^{J_{\text{tot}}M\epsilon} &= (1 + \delta_{K0})^{-1/2} \sqrt{\frac{2J_{\text{tot}} + 1}{8\pi}} \\ &\times \left[D_{K,M}^{J_{\text{tot}}*} Y_{j_1j_2}^{JK} + \epsilon(-1)^{j_1+j_2+J+J_{\text{tot}}} D_{-K,M}^{J_{\text{tot}}*} Y_{j_1j_2}^{J-K} \right], \end{aligned} \quad (4)$$

where $D_{K,M}^{J_{\text{tot}}}$ is the Wigner rotation matrix.⁵³ $Y_{j_1j_2}^{JK}$ is defined as

$$Y_{j_1j_2}^{JK} = \sum_m D_{Km}^{J_{\text{tot}}*}(0, \theta_2, \varphi) \sqrt{\frac{2j_1 + 1}{4\pi}} \langle j_2 m j_1 0 | Jm \rangle y_{j_2m}(\theta_1, 0) \quad (5)$$

and y_{j_2m} denotes the spherical harmonics. Note the restriction that $\epsilon(-1)^{j_1+j_2+J+J_{\text{tot}}} = 0$ for $K = 0$ in eqn (4).

The centrifugal-sudden (CS) approximation^{54,55} is widely employed in the quantum scattering calculations due to the significant reduction of the computational cost. It has also been proved to work well in bimolecular reactions with well-defined barriers.^{35,56–60} Under the CS approximation, the centrifugal term in the Hamiltonian, $(\hat{J}_{\text{tot}} - \hat{J})^2$, is given by

$$\begin{aligned} &\langle \Phi_{JK}^{J_{\text{tot}}M\epsilon} | (\hat{J}_{\text{tot}} - \hat{J})^2 | \Phi_{J'K'}^{J_{\text{tot}}M\epsilon} \rangle \\ &\approx \delta_{JJ'} \delta_{KK'} [J_{\text{tot}}(J_{\text{tot}} + 1) + J(J + 1) - 2K^2]. \end{aligned} \quad (6)$$

The initial wave packet $|\varphi\rangle$ is constructed as the direct product of a localized Gaussian wave packet along the scattering coordinate and a specific rovibrational state of the reactant BCD in the BF representation:

$$|\varphi\rangle = \left(\frac{1}{\pi\delta^2} \right)^{1/4} e^{-(\rho-\rho_0)^2/2\delta^2} e^{-ik_i\rho} |\nu_0 J_0 \tau; J_{\text{tot}} \epsilon\rangle, \quad (7)$$

where ρ_0 and δ are the mean position and width of the Gaussian wavepacket and k_i is the mean momentum given by E_i via $k_i = \sqrt{2\mu_\rho E_i}$. ν_0, J_0 and τ denote the initial vibrational quantum number, the initial angular momentum quantum number and the parity of the reactant BCD, respectively. The eigenstates of the reactant BCD are obtained by diagonalizing the three-dimensional

Hamiltonian:

$$\begin{aligned} \hat{H} &= -\frac{1}{2\mu_{r_1}} \frac{\partial^2}{\partial r_1^2} - \frac{1}{2\mu_{r_2}} \frac{\partial^2}{\partial r_2^2} + \frac{\hat{j}_1^2}{2\mu_1 r_1^2} + \frac{(\hat{J} - \hat{j}_1)^2}{2\mu_2 r_2^2} \\ &+ \hat{V}(\rho = \infty, r_1, r_2, \theta_1, \theta_2 = 0, \varphi = 0). \end{aligned} \quad (8)$$

The second-order split-operator method was employed in the propagation.⁶¹ To prevent artificial boundary reflection from the end of the numerical grid, the negative imaginary absorbing potentials D are applied at the grid edges:

$$D(x) = -i\alpha \left(\frac{x - x_a}{x_{\text{max}} - x_a} \right)^n, \quad (9)$$

in which $x = \rho, r_1$ and r_2 , x_a is the starting point of the absorbing potential.

The total reaction probability from a specified initial ro-vibrational state of BCD is calculated using the flux formula:

$$P_{\nu_0 J_0 \tau}^{J_{\text{tot}}\epsilon}(E) = \langle \psi_i^+(E) | \hat{F} | \psi_i^+(E) \rangle \quad (10)$$

where \hat{F} is the flux operator. The energy-dependent scattering wavefunction, $\psi_i^+(E)$, is obtained by Fourier transforming the time-dependent wavefunction at the dividing surface in the product channel. The integral cross section (ICS) from the initial state is obtained by summing the reaction probabilities over all relevant partial waves:

$$\sigma_{\nu_0 J_0 \tau}(E_c) = \frac{1}{(2J_0 + 1)} \frac{\pi}{2\mu_R E_c} \sum_{K_0\epsilon} \sum_{J_{\text{tot}} \geq K_0} (2J_{\text{tot}} + 1) P_{\nu_0 J_0 \tau K_0}^{J_{\text{tot}}\epsilon}(E_c). \quad (11)$$

In this work, the reaction probabilities for non-zero partial waves are calculated under the CS approximation. Since we are only interested in the vibrational mode specificity, no rotationally excited reactant is considered. Ideally, the reactive flux should be collected at two dividing surfaces corresponding to the cleavage of the two bonds in the reactant. Considering the indistinguishability of the two hydrogen atoms and thus the same possibility of cleavage, we just collect the reactive flux from one bond. Note that the two bonds are both allowed to be broken in the theoretical simulation. The reaction probability from a specific initial state is doubled when calculating the corresponding ICS.

IIB. Local mode representation

In the local mode representation, the symmetry-adapted local mode bases for triatomic XY_2 molecule are defined as follows:⁴⁶

$$\begin{aligned} |nm^\pm\rangle &= 2^{-1/2} (|nm\rangle \pm |mn\rangle) \quad n < m, \\ |nm^+\rangle &= |nm\rangle, \quad n = m \end{aligned} \quad (12)$$

in which the first and second quantum numbers in the bracket refer to excitations of the two XY bonds, respectively. In the $(2 + 1)$ Radau coordinates describing the reactant XY_2 (BCD in Fig. 2), $|nm\rangle$ can be approximate to the direct product of eigenfunctions of the 1D reference Hamiltonians, *i.e.*,

$$|nm\rangle = \phi_n(r_1) \phi_m(r_2). \quad (13)$$

Because the atom X (X = S, O) is much heavier than the atom Y (Y = H) in this work. Apparently, the local mode representation is suitable to describe excitations of the symmetric and anti-symmetric stretching modes. The obtained eigenfunctions $|\varphi_i\rangle$ of the three-dimensional Hamiltonian of BCD are expressed as

$$|\varphi_i\rangle = \sum_{nmj} c_{nmj} |nmj\rangle = \sum_{nmj} c_{nm} c_j |nm\rangle |j\rangle, \quad (14)$$

in which j denotes the angular basis index. Thus, the square of the coefficients $|c_{nm}|^2$ is calculated by summing the square of c_{nmj} over all angular bases. If one is only interested in the excitations of the stretching modes and in this case the reactant is always in the ground state of the bending mode, the i th eigenfunction is expanded in terms of the local mode wavefunction $|nm\rangle$ as

$$|\varphi_i\rangle = \sum_{nm} c_{nm} |nm\rangle |\nu_b = 0\rangle, \quad (15)$$

in which ν_b denotes excitation in the bending mode. The angular distribution of $|\varphi_i\rangle$ can be reasonably considered to be the same as that of the ground state $|\varphi_0\rangle$. Then, the

expansion coefficients are approximately computed by

$$c_{nm}^i = \sum_j \langle 00; j | nm; j \rangle_i, \quad (16)$$

in which j labels the angular basis. Actually, the square of c_{nm} calculated by eqn (16) is almost equal to the corresponding one by eqn (14). However, one cannot get the sign of c_{nm} by eqn (14).

III. Results and discussion

The numerical parameters employed in the quantum dynamics calculations are given in Table 1. The expansion coefficients of interested eigenstates of H₂S and H₂O on the local mode wavefunction $|nm\rangle$ are, respectively, listed in Tables 2 and 3, with which these states can be easily assigned in the local mode representation. In Table 2, the calculated energies of H₂S agree well with the experimental values. According to the expansion coefficients, each state can be clearly assigned in the local mode representation except the (200) state. The state (200) is expanded as $|200\rangle = 0.6995|02\rangle + 0.6995|20\rangle + 0.1277|11\rangle$ and thus approximately labeled as $|02^+\rangle$. Table 3 shows that the calculated energies of H₂O are in good consistent with the experimental values as well. Since the local mode character of

Table 1 Numerical parameters used in the wave packet calculations (atomic units are used unless stated otherwise)

	H + H ₂ S	H + H ₂ O
Grid/basis range and size:	$R \in [1.2, 12.5]$ $r_1, r_2 \in [1.5, 7.8]$ $N_R^{\text{tot}} = 66, N_R^{\text{int}} = 46$ $N_{r_1}^{\text{int}} = 42, N_{r_1}^{\text{asy}} = 5$ $N_{r_2}^{\text{int}} = 24, N_{r_2}^{\text{asy}} = 5$ $j_{1\text{max}} = 68, j_{2\text{max}} = 24$	$R \in [1.0, 12.5]$ $r_1, r_2 \in [1.0, 5.5]$ $N_R^{\text{tot}} = 104, N_R^{\text{int}} = 40$ $N_{r_1}^{\text{int}} = 32, N_{r_1}^{\text{asy}} = 5$ $N_{r_2}^{\text{int}} = 32, N_{r_2}^{\text{asy}} = 5$ $j_{1\text{max}} = 32, j_{2\text{max}} = 32$
Initial wave packet:	$R_0 = 10.0, \delta = 0.3, E_0 = 0.65 \text{ eV}$	$R_0 = 8.5, \delta = 0.35, E_0 = 0.45 \text{ eV}$
Absorbing potential:	$R_a = 10.0, \alpha_R = 0.075, n_R = 2.5$ $r_{1a} = 6.1, \alpha_{r_1} = 0.050, n_{r_1} = 2.0$ $r_{1a} = 4.1, \alpha_{r_1} = 0.050, n_{r_1} = 2.0$	$R_a = 9.0, \alpha_R = 0.075, n_R = 3.0$ $r_{1a} = 3.1, \alpha_{r_1} = 0.035, n_{r_1} = 2.0$ $r_{1a} = 3.1, \alpha_{r_1} = 0.035, n_{r_1} = 2.0$
Flux position:	$r_1^F = 6.0$	$r_1^F = 2.6$
Propagation time	25 000	12 000

Table 2 Calculated vibrational energies in cm⁻¹ of the excited states of symmetric and antisymmetric stretching modes of H₂S and the expansion coefficients of the corresponding eigenfunctions on the local mode wavefunction $|nm\rangle$, where n and m denote S–H local-mode quantum numbers

			Projection									
Normal	Cal	Obs ^a	01⟩	10⟩	02⟩	20⟩	11⟩	03⟩	30⟩	12⟩	21⟩	Local
(100)	2615.12	2614.41	0.7060	0.7060								01 ⁺ ⟩
(001)	2627.35	2628.46	0.7067	−0.7067								01 [−] ⟩
(200)	5145.69	5145.12			0.6995	0.6995	0.1277					02 ⁺ ⟩
(101)	5147.43	5147.36			0.7057	−0.7057						02 [−] ⟩
(002)	5242.58						0.9896					11 ⁺ ⟩
(300)	7578.54	7576.3						0.7033	0.7033			03 ⁺ ⟩
(201)	7578.83	7576.3						0.7037	−0.7037			03 [−] ⟩
(102)	7754.03	7751.9								0.7029	0.7029	12 ⁺ ⟩
(003)	7778.84	7779.2								0.7040	−0.7040	12 [−] ⟩

^a See <http://cccbdb.nist.gov>.

Table 3 Calculated vibrational energies in cm^{-1} of the excited states of symmetric and antisymmetric stretching modes of H_2O and the expansion coefficients of the corresponding eigenfunctions on the local mode wavefunction $|nm\rangle$, where n and m denote O–H local-mode quantum numbers

			Projection									
Normal	Cal	Obs ^a	01⟩	10⟩	02⟩	20⟩	11⟩	03⟩	30⟩	12⟩	21⟩	Local
(100)	3657.90	3657	0.7047	0.7047								01 ⁺ ⟩
(001)	3754.65	3756	0.7055	0.7055								01 [−] ⟩
(200)	7204.03	7201			0.6359	0.6359	0.4193					02 ⁺ ⟩
(101)	7251.32	7250			0.7019	−0.7019						02 [−] ⟩
(002)	7444.39	7445			0.2967	0.2967	−0.8996			0.2401	0.2401	11 ⁺ ⟩
(300)	10605.91							0.6610	0.6610	0.2187	0.2187	03 ⁺ ⟩
(201)	10618.77	10 613						0.6857	0.6857	0.1227	0.1227	03 [−] ⟩
(102)	10872.05							−0.2171	−0.2171	0.6625	0.6625	12 ⁺ ⟩
(003)	11033.76	11 032						0.1220	0.1220	0.6858	0.6858	12 [−] ⟩

^a See <http://cccbdb.nist.gov>.

H_2O is not as strong as that of H_2S , some eigenstates are no longer pure states in the local mode representation. Thus, the assignments of these states in the local mode representation are approximate. Interestingly, the state (101) in the normal mode representation corresponds well to the state $|02^-\rangle$ in the local mode representation.

Fig. 3 shows the calculated integral cross sections (ICSSs) of the abstraction reaction $\text{H} + \text{H}_2\text{S} \rightarrow \text{H}_2 + \text{SH}$, for which the symmetric and/or antisymmetric stretching modes of the reactant H_2S are excited up to second overtones. The initial states are assigned in both the normal mode representation and the local mode representation. The symmetry-adapted local mode bases for the XY_2 -like molecules are defined as $|nm^\pm\rangle = 2^{-1/2}(|nm\rangle \pm |nm\rangle)$, $n < m$; $|nm^+\rangle = 2^{-1/2}|nm\rangle$, $n = m$, in which the first and second quantum numbers n and m denote excitations of the two XY bonds, respectively.⁴⁶ From Fig. 3, it can be seen that the ICSSs of exciting the state (200) differ visibly from

the state (002) while they are almost identical to those of exciting the state (101). This behavior is incomprehensible according to the concerted motions of involving atoms of these normal modes. In the local mode representation, the three excited states (200), (101), and (002) are labeled as the states $|02^+\rangle$, $|02^-\rangle$, and $|11^+\rangle$, respectively. From the viewpoint of the local mode, both the states $|02^+\rangle$ and $|02^-\rangle$ can be approximately considered to be individual two-quanta excitation of the two SH bonds while the state $|11^+\rangle$ to be synergistic one-quantum excitations of the two SH bonds. Due to the direct mechanism of the abstraction reaction and the negligible inter-bond coupling between the two SH bonds of H_2S , excitations of the initial states $|02^+\rangle$ and $|02^-\rangle$ would promote reasonably the reaction with equivalent efficacies. The similar reactivities are also expected for exciting the states $|03^+\rangle$ and $|03^-\rangle$, corresponding to the states (300) and (201) in the normal mode representation. Clearly, the ICSSs from the two states $|03^+\rangle$ and $|03^-\rangle$ are almost indistinguishable. Furthermore, exciting the state $|12^+\rangle$ gives ICSSs resembling the counterparts of exciting the state $|12^-\rangle$. For the abstraction reaction $\text{H} + \text{H}_2\text{O} \rightarrow \text{H}_2 + \text{OH}$, as aforementioned, Fu *et al.*³² observed that exciting the state (200) of the reactant H_2O promotes the reactivity much more than exciting the state (002) while its efficiency is comparable to that of exciting the state (101). The assignments of the three initial states of H_2O in the local mode representation are the same as those of H_2S and therefore can be used to explain the observed dynamics behavior.

Fig. 4 shows the calculated ICSSs of the exchange channel $\text{H}' + \text{H}_2\text{S} \rightarrow \text{H}'\text{SH} + \text{H}$. Clearly, the ICSSs from the state (101) are nearly indistinguishable from the ICSSs from the state (200). The two states (101) and (200) are assigned in the local mode representation as $|02^-\rangle$ and $|02^+\rangle$, respectively. Similarly, the initial state $|03^-\rangle$ gives ICSSs very close to the $|03^+\rangle$. In addition, the ICSSs from $|12^-\rangle$ is comparable to the ICSSs from $|12^+\rangle$. The mode specificities in the exchange channel can be well explained in the local mode representation according to the strong local mode character as well.

Intramolecular vibrational redistribution (IVR) plays an important role in molecular reaction dynamics. Chemists always hope to insert a chemically significant amount of energy in one bond and keep it there for a chemically relevant time,

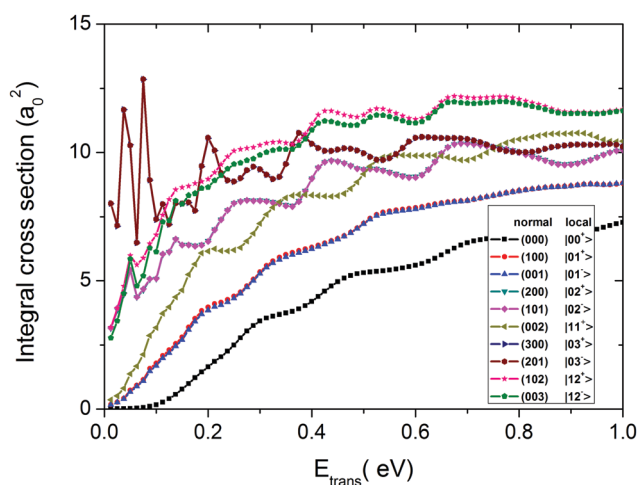


Fig. 3 Calculated integral cross sections of the abstraction reaction $\text{H} + \text{H}_2\text{S} \rightarrow \text{H}_2 + \text{SH}$ from the ground, fundamental, first and second overtones and combination bands of the symmetric and antisymmetric stretching modes of the reactant H_2S . The numbers (n_1, n_2, n_3) in the normal mode representation denote excitations in the symmetric stretching mode, the bending mode and the antisymmetric stretching mode. The numbers (n, m) in the local mode representation refer to excitations in the two SH bonds.

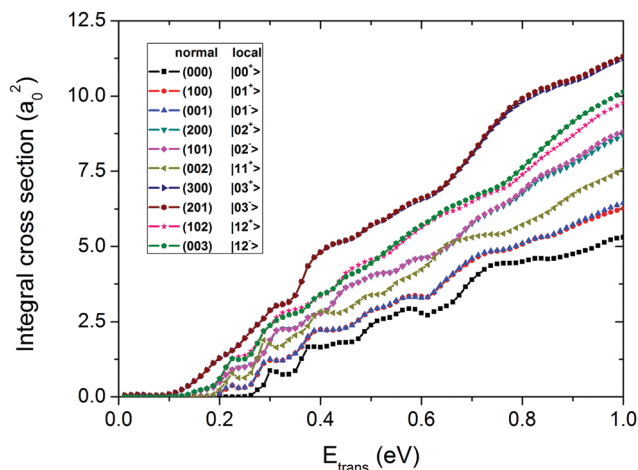


Fig. 4 Calculated integral cross sections of the exchange reaction $\text{H}' + \text{H}_2\text{S} \rightarrow \text{H}'\text{SH} + \text{H}$ from the ground, fundamental, first and second overtones and combination bands of the symmetric and antisymmetric stretching modes of the reactant H_2S .

so as to manipulate chemical reactivity. Local mode molecules would be good candidates for realizing chemists' dream. To this end, one component in the local mode representation is extracted from the initial wave packet to propagate, mimicking individual excitation of one chemical bond. Fig. 5 displays the

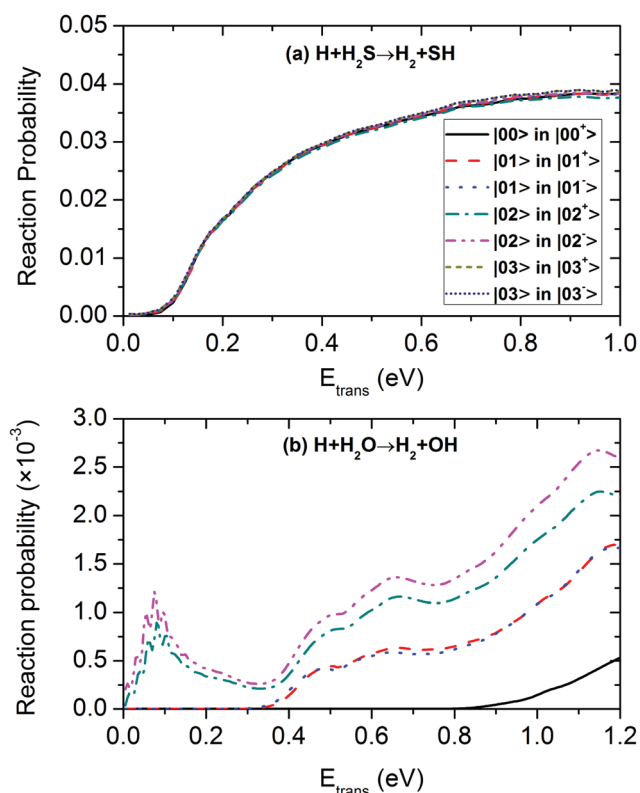


Fig. 5 Calculated reaction probabilities of the abstraction reactions from one component of the $|00^+\rangle$, $|01^+\rangle$, $|01^-\rangle$, $|02^+\rangle$, $|02^-\rangle$, $|03^+\rangle$ and $|03^-\rangle$ states of the reactants H_2S and H_2O . (a) $\text{H} + \text{H}_2\text{S} \rightarrow \text{H}_2 + \text{SH}$; (b) $\text{H} + \text{H}_2\text{O} \rightarrow \text{H}_2 + \text{OH}$.

calculated reaction probabilities of the abstraction reactions $\text{H} + \text{H}_2\text{S} \rightarrow \text{H}_2 + \text{SH}$ and $\text{H} + \text{H}_2\text{O} \rightarrow \text{H}_2 + \text{OH}$. For the sake of discussion, the reaction probability thereafter is calculated by cumulating only the reaction flux resulting from the breaking of the first bond associated with the quantum n in a state $|nm^+\rangle$, *i.e.*, passing through one transition state. Note that in the figure “ $|00\rangle$ in $|00^+\rangle$ ” means $\sqrt{2}/2$ of the wave function $|00^+\rangle$ is taken to propagate. Impressively, the vibrational energy initially deposited in one SH bond of H_2S is entirely quenched and therefore excitation of one bond has no visible effect on the cleavage of the other bond. For the reactant H_2O , the local mode character is slightly weaker than the molecule H_2S . However, the IVR in H_2O appears to be much stronger. The vibrational energy initially deposited in one OH bond can flow into the other bond to promote the breaking of the bond. In sharp contrast to the abstraction reaction between H and H_2S , the breaking of one OH bond is significantly enhanced by exciting the other OH bond in the reactant H_2O .

The dynamics of bimolecular chemical reactions is sometimes not uniquely dominated by the intramolecular interaction. The intermolecular interaction has been proved to modulate the reaction in an unpredictable way.^{2,13,17,62–64} The abstraction reaction usually has a well-defined barrier and occurs directly while the exchange reaction often takes place *via* a well and becomes indirect and slow. Fig. 6 depicts the

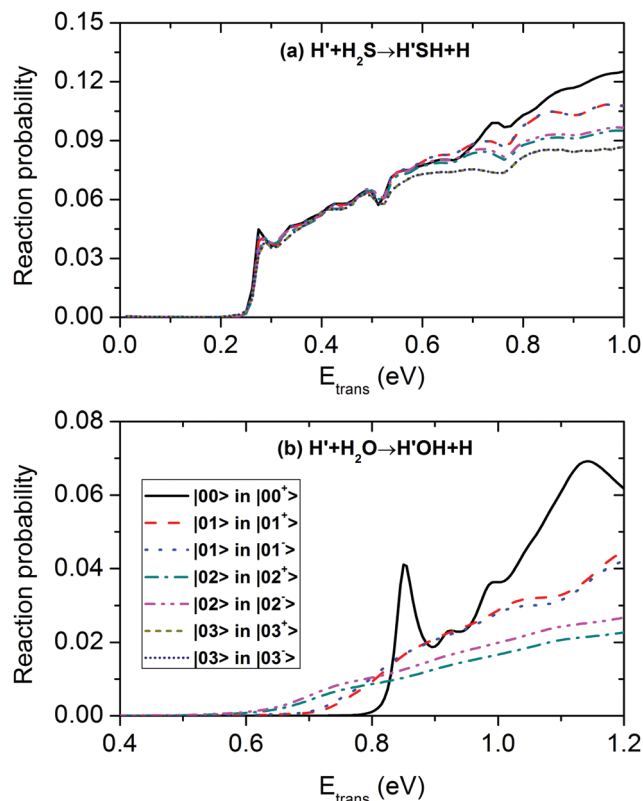


Fig. 6 Calculated reaction probabilities of the exchange reactions from one component of the $|00^+\rangle$, $|01^+\rangle$, $|01^-\rangle$, $|02^+\rangle$, $|02^-\rangle$, $|03^+\rangle$ and $|03^-\rangle$ states of the reactants H_2S and H_2O . (a) $\text{H}' + \text{H}_2\text{S} \rightarrow \text{H}'\text{SH} + \text{H}$; (b) $\text{H}' + \text{H}_2\text{O} \rightarrow \text{H}'\text{OH} + \text{H}$.

calculated reaction probabilities of the exchange reactions between H and H₂S and H₂O from the first component of the states $|00^+\rangle$, $|01^+\rangle$, $|01^-\rangle$, $|02^+\rangle$, $|02^-\rangle$, $|03^+\rangle$ and $|03^-\rangle$. For the reaction $H' + H_2S \rightarrow H'SH + H$, the reaction probabilities from different states are close to each other at low collision energies, indicating that exciting one SH bond has negligible effect on the other SH bond. However, at high collision energies, the reaction probability decreases with the increase of the initial quantum number of the reactant H₂S. For the reaction $H' + H_2O \rightarrow H'OH + H$, the cleavage of one OH bond is hindered by exciting the other OH bond at high collision energies while it is enhanced at low collision energies. Thus, exciting one SH (OH) bond suppresses the cleavage of the other SH (OH) bond in H₂S (H₂O) at relatively high collision energies. On the other hand, the vibrational energy in one SH bond cannot flow into the other bond at low collision energies and yet the vibration energy in one OH bond enhances the breaking of the other OH bond. In addition, the energy flow between the two OH bonds is obviously more serious than that between the two SH bonds in the exchange reactions. By comparison with what has been observed in the abstraction reaction above, it implies that there exist competitions between the intra-molecular interaction and the intermolecular interaction. The intramolecular interaction generally dominates direct reactions while the intermolecular interaction plays an important role in indirect reactions.

A key point of bond-selective chemistry is to look for long-lived vibrational eigenstates of a single bond. The lifetime of such vibrational states in real molecules is closely related to IVR. When a reactant molecule is excited to highly vibrational state, the vibrational energy starts to transfer among different modes even though the reaction does not take place. If the inter-bond coupling is negligible, there would exist a long-lived vibrational state of a single bond. In this case, each bond eigenfunction is expected to have independent contribution to the reaction. Fig. 7 shows the calculated reaction probabilities of the abstraction reactions from the state $|02^-\rangle$. In the local mode representation, $|02^-\rangle$ is approximate to be the sum of $2^{-1/2}|02\rangle$ and $-2^{-1/2}|20\rangle$, in which the two components mimic the vibrational eigenstates of the two bonds. The probabilities from each component of the eigenfunction $|02^-\rangle$ are plotted in the same figure, together with the sum of them. For the $H + H_2S \rightarrow H_2 + SH$ reaction, the reaction probability from the state $|02^-\rangle$ is almost equal to the sum of the reaction probabilities from the two components $2^{-1/2}|02\rangle$ and $-2^{-1/2}|20\rangle$ over the energy range interested. The feature implies that the two states $|02\rangle$ and $|20\rangle$, associated with the two SH bonds, are independent in the reaction process. Remind of what has been clarified in Fig. 5 that the vibrational energy initially deposited in one SH bond cannot flow into the other SH bond, the two states $|02\rangle$ and $|20\rangle$ are both very good local mode eigenstates suitable for dynamics studies in the bond-selective chemistry. For the $H + H_2O \rightarrow H_2 + OH$ reaction, the reaction probability from the state $|02^-\rangle$ differs visibly from the sum from the two components, indicating that the coherence between the two local mode states $|02\rangle$ and $|20\rangle$ is destroyed in

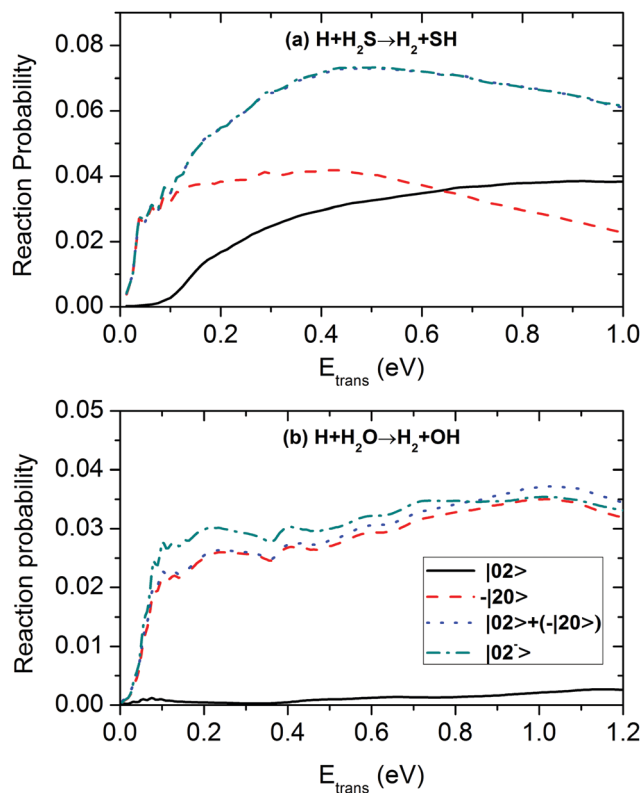


Fig. 7 Calculated reaction probabilities of the abstraction reactions from the $|02^-\rangle$ states of the reactants H₂S and H₂O. The sum of the reaction probabilities from each component is also shown for comparison. (a) $H + H_2S \rightarrow H_2 + SH$; (b) $H + H_2O \rightarrow H_2 + OH$.

the reaction. In addition, the $|20\rangle$ state predominates the abstraction reaction between H and H₂S at low collision energies while it controls the reaction between H and H₂O over the whole energy range.

The reaction probabilities of the exchange reactions, as shown in Fig. 8, present similar features to the abstraction reactions. For the reaction $H' + H_2S \rightarrow H'SH + H$, the sum of the reaction probabilities from the two components of the state $|02^-\rangle$ is nearly equal to that from the whole state $|02^-\rangle$ although the conformity is not as good as in the abstraction reaction $H + H_2S \rightarrow H_2 + SH$ in the moderate energy range. For the reaction $H' + H_2O \rightarrow H'OH + H$, the sum of the probabilities from the two components of the state $|02^-\rangle$ is visibly smaller than from the whole state $|02^-\rangle$.

According to the Morse oscillator model proposed by Watson *et al.*⁶⁵ and developed in more detail by Child and Lawton⁶⁶ and Mortensen *et al.*,⁶⁷ in which a local mode parameter is introduced to give an indication of local or normal mode character, the local mode ranking is $H_2S > H_2Se > CH_2Cl_2 > H_2O > C_2H_2 > D_2O > C_2D_2 > SO_2$ for XY₂-like molecules, $SiH_3D > CH_3D > NH_3 > SiHD_3 > CHD_3$ for XY₃-like molecules and $SiH_4 > CH_4 > SiD_4 > CD_4$ for XY₄-like molecules with H₂S, SiH₃D and SiH₄ very close to the local mode limit.⁴⁶ In general, the reactions involving molecules with strong local mode character favor local mode description while others prefer normal mode description. The strong local mode

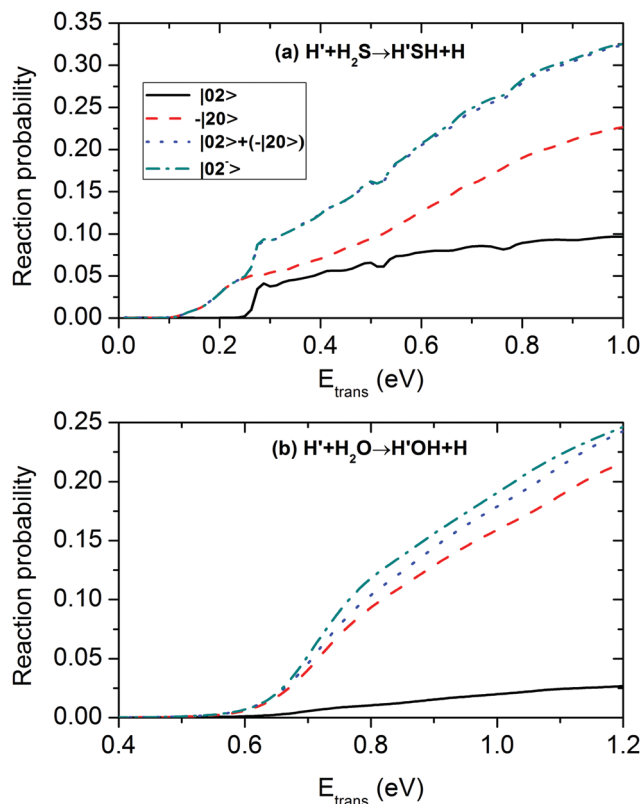


Fig. 8 Calculated reaction probabilities of the exchange reactions from the $|02^- \rangle$ states of the reactants H_2S and H_2O . The sum of the reaction probabilities from each component is also shown for comparison. (a) $\text{H}' + \text{H}_2\text{S} \rightarrow \text{H}'\text{SH} + \text{H}$; (b) $\text{H}' + \text{H}_2\text{O} \rightarrow \text{H}'\text{OH} + \text{H}$.

character of the reactant H_2S definitely results in the observed interesting dynamics behavior in the reaction between H and H_2S . In sharp contrast, although the local mode character of the reactant H_2O is slightly weaker than the reactant H_2S , the reaction dynamics between H and H_2O differs dramatically from the reaction between H and H_2S . The interbond coupling is possibly caused by the potential energy coupling, the kinetic energy coupling or both. For the molecule H_2O , the interbond coupling is roughly equally attributed to the potential energy term and the kinetic energy term. However, when the two types of contribution have opposite signs, as in the molecule H_2S , the interbond coupling would be negligible due to the nearly exact cancellation.⁴⁶ It may be interesting to explore the effect of the potential energy coupling and the kinetic energy coupling on the reaction dynamics separately. Nevertheless, it is beyond the scope of this work.

IV. Conclusions

The mode-specific dynamics of the reactions between the hydrogen atom and the molecules H_2S and H_2O has been studied using a full-dimensional quantum scattering model. The $(2+1)$ Radau–Jacobi coordinates are adopted to introduce local mode descriptions of the reactant molecules. The mode specificities that are difficult to understand in normal mode

representation are well rationalized in the local mode representation. There exist competitions between intramolecular interaction and intermolecular interaction on affecting the dynamics of bimolecular reactions. For the typical local mode molecule H_2S , the intramolecular vibrational redistribution is negligible, resulting in no visible energy flow between the two SH bonds in the direct abstraction reaction between H and H_2S . However, the intermolecular interaction that is expected to be significant in the exchange reaction leads to notable dynamics effect at high collision energies. Since the local mode character of the molecule H_2O is not as strong as in the molecule H_2S , the energy flow between the two OH bonds appears to be prevalent in the reaction between H and H_2O .

Conflicts of interest

There are no conflicts to declare.

Acknowledgements

This work was supported by the National Natural Science Foundation of China (Projects No. 21603266 to H. Song and 21773297 to M. Yang).

References

- H. Guo and K. Liu, *Chem. Sci.*, 2016, **7**, 3992–4003.
- T. Westermann, J. B. Kim, M. L. Weichman, C. Hock, T. I. Yacovitch, J. Palma, D. M. Neumark and U. Manthe, *Angew. Chem., Int. Ed.*, 2014, **53**, 1122–1126.
- D. H. Zhang and H. Guo, *Annu. Rev. Phys. Chem.*, 2016, **67**, 135–158.
- J. M. Bowman and P. L. Houston, *Chem. Soc. Rev.*, 2017, **46**, 7615–7624.
- R. N. Zare, *Science*, 1998, **279**, 1875–1879.
- F. F. Crim, *Acc. Chem. Res.*, 1999, **32**, 877–884.
- F. F. Crim, *Proc. Natl. Acad. Sci. U. S. A.*, 2008, **105**, 12654–12661.
- T. Wang, J. Chen, T. Yang, C. Xiao, Z. Sun, L. Huang, D. Dai, X. Yang and D. H. Zhang, *Science*, 2013, **342**, 1499–1502.
- T. Yang, J. Chen, L. Huang, T. Wang, C. Xiao, Z. Sun, D. Dai, X. Yang and D. H. Zhang, *Science*, 2015, **347**, 60–63.
- K. Liu, *Annu. Rev. Phys. Chem.*, 2016, **67**, 91–111.
- Q. Guo, C. Zhou, Z. Ma, Z. Ren, H. Fan and X. Yang, *Annu. Rev. Phys. Chem.*, 2016, **69**, 451–472.
- D. H. Zhang, M. A. Collins and S.-Y. Lee, *Science*, 2000, **290**, 961–963.
- G. Czako and J. M. Bowman, *Science*, 2011, **334**, 343–346.
- J. Yang, D. Zhang, B. Jiang, D. Dai, G. Wu, D. Zhang and X. Yang, *J. Phys. Chem. Lett.*, 2014, **5**, 1790–1794.
- H. Guo and B. Jiang, *Acc. Chem. Res.*, 2014, **47**, 3679–3685.
- J. Li, B. Jiang, H. Song, J. Ma, B. Zhao, R. Dawes and H. Guo, *J. Phys. Chem. A*, 2015, **119**, 4667–4687.
- Y. Wang, H. Song, I. Szabó, G. Czako, H. Guo and M. Yang, *J. Phys. Chem. Lett.*, 2016, **7**, 3322–3327.

- 18 H. Song, M. Yang and H. Guo, *J. Chem. Phys.*, 2016, **145**, 131101.
- 19 B. Fu, X. Shan, D. H. Zhang and D. C. Clary, *Chem. Soc. Rev.*, 2017, **46**, 7625–7649.
- 20 G. Nyman and D. C. Clary, *J. Chem. Phys.*, 1994, **101**, 5756–5771.
- 21 T. Takayanagi, *J. Chem. Phys.*, 1996, **104**, 2237–2242.
- 22 G. Nyman, H.-G. Yu and R. B. Walker, *J. Chem. Phys.*, 1998, **109**, 5896–5904.
- 23 H.-G. Yu and G. Nyman, *J. Chem. Phys.*, 1999, **110**, 7233–7244.
- 24 J. Palma and D. C. Clary, *J. Chem. Phys.*, 2000, **112**, 1859–1867.
- 25 H. G. Yu, *J. Chem. Phys.*, 2001, **114**, 2967–2976.
- 26 M. Yang, D. H. Zhang and S.-Y. Lee, *J. Chem. Phys.*, 2002, **117**, 9539–9542.
- 27 M. Yang, S.-Y. Lee and D. H. Zhang, *J. Chem. Phys.*, 2007, **126**, 064303.
- 28 B. Fu and D. H. Zhang, *J. Phys. Chem. A*, 2011, **116**, 820–825.
- 29 R. Liu, H. Xiong and M. Yang, *J. Chem. Phys.*, 2012, **137**, 174113.
- 30 R. Liu, M. Yang, G. Czako, J. M. Bowman, J. Li and H. Guo, *J. Phys. Chem. Lett.*, 2012, **3**, 3776–3780.
- 31 F. Meng, W. Yan and D. Wang, *Phys. Chem. Chem. Phys.*, 2012, **14**, 13656–13662.
- 32 B. Fu and D. H. Zhang, *J. Chem. Phys.*, 2013, **138**, 184308.
- 33 B. Jiang and H. Guo, *J. Am. Chem. Soc.*, 2013, **135**, 15251–15256.
- 34 J. Li, B. Jiang and H. Guo, *J. Am. Chem. Soc.*, 2013, **135**, 982–985.
- 35 H. Song, S.-Y. Lee, M. Yang and Y. Lu, *J. Chem. Phys.*, 2013, **139**, 154310.
- 36 D. Wang and G. Czako, *J. Phys. Chem. A*, 2013, **117**, 7124–7130.
- 37 R. Welsch and U. Manthe, *J. Chem. Phys.*, 2014, **141**, 174313.
- 38 R. Welsch and U. Manthe, *J. Chem. Phys.*, 2014, **141**, 051102.
- 39 H. Song and H. Guo, *J. Phys. Chem. A*, 2015, **119**, 6188–6194.
- 40 J. Espinosa-Garcia, C. Rangel and J. C. Corchado, *Theor. Chem. Acc.*, 2015, **135**, 1–8.
- 41 N. Liu and M. Yang, *J. Chem. Phys.*, 2015, **143**, 134305.
- 42 J. Qi, H. Song, M. Yang, J. Palma, U. Manthe and H. Guo, *J. Chem. Phys.*, 2016, **144**, 171101.
- 43 S. Liu and D. H. Zhang, *Chem. Sci.*, 2016, **7**, 261–265.
- 44 B. Zhao, Z. Sun and H. Guo, *J. Am. Chem. Soc.*, 2015, **137**, 15964–15970.
- 45 B. Zhao, Z. Sun and H. Guo, *Phys. Chem. Chem. Phys.*, 2018, **20**, 191–198.
- 46 M. S. Child and L. Halonen, *Advances in Chemical Physics*, John Wiley & Sons, Inc., 2007, pp. 1–58, , DOI: 10.1002/9780470142813.ch1.
- 47 J. Li, B. Jiang and H. Guo, *J. Chem. Phys.*, 2013, **139**, 204103.
- 48 D. Lu and J. Li, *J. Chem. Phys.*, 2016, **145**, 014303.
- 49 B. Jiang and H. Guo, *J. Chem. Phys.*, 2013, **139**, 054112.
- 50 M. Yang, D. H. Zhang, M. A. Collins and S.-Y. Lee, *J. Chem. Phys.*, 2001, **115**, 174–178.
- 51 J. Chen, X. Xu and D. H. Zhang, *J. Chem. Phys.*, 2013, **138**, 154301.
- 52 D. H. Zhang and J. Z. H. Zhang, *J. Chem. Phys.*, 1993, **99**, 5615–5618.
- 53 R. N. Zare, *Angular Momentum*, Wiley, New York, 1988.
- 54 R. T. Pack, *J. Chem. Phys.*, 1974, **60**, 633–639.
- 55 P. McGuire and D. J. Kouri, *J. Chem. Phys.*, 1974, **60**, 2488–2499.
- 56 D. H. Zhang and S. Y. Lee, *J. Chem. Phys.*, 1999, **110**, 4435–4444.
- 57 U. Manthe and F. Matzkies, *J. Chem. Phys.*, 2000, **113**, 5725–5731.
- 58 D. H. Zhang, M. Yang and S.-Y. Lee, *J. Chem. Phys.*, 2002, **117**, 10067–10072.
- 59 F. Huarte-Larrañaga and U. Manthe, *J. Chem. Phys.*, 2003, **118**, 8261–8267.
- 60 H. Song, Y. Lu and S.-Y. Lee, *J. Chem. Phys.*, 2012, **136**, 114307.
- 61 J. A. Fleck, Jr., J. R. Morris and M. D. Feit, *Appl. Phys.*, 1976, **10**, 129–160.
- 62 Z. Zhang, Y. Zhou, D. H. Zhang, G. Czako and J. M. Bowman, *J. Phys. Chem. Lett.*, 2012, **3**, 3416–3419.
- 63 J. Li, B. Jiang and H. Guo, *Chem. Sci.*, 2013, **4**, 629–632.
- 64 J. Yang, K. Shao, D. Zhang, Q. Shuai, B. Fu, D. H. Zhang and X. Yang, *J. Phys. Chem. Lett.*, 2014, **5**, 3106–3111.
- 65 I. A. Watson, B. R. Henry and I. G. Ross, *Spectrochim. Acta, Part A*, 1981, **37**, 857–865.
- 66 M. S. Child and R. T. Lawton, *Faraday Discuss. Chem. Soc.*, 1981, **71**, 273–285.
- 67 O. S. Mortensen, B. R. Henry and M. A. Mohammadi, *J. Chem. Phys.*, 1981, **75**, 4800–4808.